Available online at www.sciencedirect.com

SciVerse ScienceDirect

Journal of the European Ceramic Society 33 (2013) 2625–2631

www.elsevier.com/locate/jeurceramsoc

Synthesis of nanostructured Nd:Y_2O_3 powders by carbonate-precipitation process for Nd:YAG ceramics

Yongfei Liu, Xiaoying Qin*, Hongxing Xin, Chunjun Song

Key Laboratory of Materials Physics, Institute of Solid State Physics, Chinese Academy of Sciences, Hefei 230031, PR China

Received 31 October 2012; received in revised form 26 April 2013; accepted 29 April 2013
Available online 28 May 2013

Abstract

Neodymium doped yttria (Nd:Y_2O_3) nanopowders were synthesized by a co-precipitation method, and the effect of thermal decomposition behavior of the precursors were studied. Nonlinear and linear heating schedules (NHS and LHS) were adopted during the calcination processes. The results show that as compared to the LHS the NHS can not only lower the crystallization temperature substantially, but also decrease the mean particle size and lighten the particle agglomeration in the obtained Nd:Y_2O_3 nanopowders. Using the obtained well-dispersed Nd:Y_2O_3 and commercial Al_2O_3 powders, transparent Nd:YAG ceramics were fabricated at 1750 °C in vacuum. Better transparency can be obtained by using the Nd:Y_2O_3 powders calcined in the NHS instead of the LHS.

Keywords: Yttria; Co-precipitation; Calcination; Agglomeration; Morphology

1. Introduction

Yttria, with its excellent properties, including a high melting point (2425 °C), optical transparency over a wide wavelength region, and high corrosion resistance, has aroused increased interest in optical applications, such as ceramic lasers.[1–3] As compared with single crystals, transparent ceramics can be produced in larger volumes and at a low cost, and can be heavily and homogeneously doped with laser-active ions.[4] However, fabrication of high transparency ceramics requires 100% density to form a pore-free microstructure. The densification of ceramics is determined by the microstructure of the green body (such as the grain size and morphology, particle size distribution (PSD), the average sizes of agglomerates and pores), rather than individual particles.[5] Generally, a well sinterable powder with a small particle size, narrow PSD, and low-agglomeration is crucial for the fabrication of Nd:Y_2O_3 or Nd:YAG transparent ceramics.

Various methods have been explored to get the optimum conditions of synthesizing yttria nanopowders, such as sol–gel combustion,[6,7] hydrothermal synthesis[8] and co-precipitation.[9,10] Among these methods, it is generally agreed that the co-precipitation is probably the most effective route to synthesize Nd:Y_2O_3 powders. Previous efforts have mainly focused on the effect of synthesis conditions[9,11] on particle characteristics. However, the thermal decomposition behavior of the precursor, which also strongly impacts the characteristics of the powders involving the particle agglomeration and PSD, is not still paid enough attention. The precursor calcination process generally includes four stages: the water removal stage, the decomposition stage, the crystallization stage and the agglomeration stage at high temperatures.[12] Moreover, in the case of complex salts, the decomposition stage can be divided into two steps: the intermediate formation in a low temperature zone and the final product generation in a high temperature zone.[13] Based on this consideration, a nonlinear heating schedule has been explored recently in the synthesis of well-dispersed YSZ nanopowders[12] by controlling the calcination parameters in each stage. The nonlinear calcination mode can be expressed as: (1) a maximum heating rate is selected to produce an intermediate substance; (2) a slow heating schedule provides the best temperature-time condition to form crystallites; (3) a relatively high heating rate is used for crystallization completion.

The objective of this study is to synthesize well-dispersed Nd:Y_2O_3 nanopowders by optimizing the calcination schedule of the precursors. Therefore, the effect of the calcination mode on morphology, PSD and agglomeration of Nd:Y_2O_3 powders

* Corresponding author. Tel.: +86 551 65592750; fax: +86 551 65591434.
E-mail address: xyqin@issp.ac.cn (X.Y. Qin).

0955-2219/$ – see front matter © 2013 Elsevier Ltd. All rights reserved.
http://dx.doi.org/10.1016/j.jeurceramsoc.2013.04.029

are discussed. After optimization of processing parameters, Nd:YAG ceramics have been obtained by the solid state reaction in vacuum at 1750 °C by using the synthesized Nd:Y_2O_3 and commercial Al_2O_3 powders as starting materials.

2. Experimental procedures

Coarse yttria (Y_2O_3, 99.99%), neodymia (Nd_2O_3, 99.99%), ammonium hydrogen carbonate (NH_4HCO_3, ACS grade), ammonium sulfate ($(NH_4)_2SO_4$, ACS grade) and nitric acid (HNO_3, semiconductor grade) were used as raw materials and provided by Aladdin-Reagent (China). First, $Y(NO_3)_3$ and $Nd(NO_3)_3$ solutions were prepared by dissolving the coarse yttria and neodymia powders in the dilute nitric acid solution respectively, and were mixed together in proportion to molar ratio of 1 at.% Nd:Y_2O_3. Then 1.5 M NH_4HCO_3 solution was dripped slowly into the mixed salt nitrate solution until the final solution pH reaches 7.5 by adding $(NH_4)_2SO_4$ (5 mol% of the yttrium) as the dispersant. The precursor was then washed with deionized water and alcohol thoroughly, following by drying at 80 °C for 24 h in an oven. Finally, the precursor was calcined at 900, 1000 and 1100 °C to obtain Nd:Y_2O_3 nanopowders via two calcination modes, linear heating schedule (LHS) and nonlinear heating schedule (NHS), which were used to examine their influences on the characteristics of the powders.

The as-prepared Nd:Y_2O_3 nanopowders were blended with commercial Al_2O_3 nanopowders (AKP-30, Sumitomo Chemical Co., Ltd.) by ball milling, with 0.5 wt% tetraethyl orthosilicate (TEOS) added as sintering aid. The mixed powders were pressed into pellets and then sintered at 1750 °C for 10 h in vacuum.[14]

The morphologies of the precursors, the Nd:Y_2O_3 nanopowders, and the Nd:YAG ceramics were examined by scanning electron microscopy (SEM, Sirion 200). The precursors were also characterized by thermal gravimetric analysis (TGA, Pyris Diamond). The particle size and PSD of Nd:Y_2O_3 nanopowders were measured by a laser particle size analyzer (Mastersizer, Malvern), and the specific surface area and the pore size distribution were measured by the BET and BJH method (Omnisorp 100CX) respectively, using nitrogen as an absorbate. The equivalent particle size (D_{BET}) could be calculated form BET surface area based on the following formula,

$$D_{BET} = \frac{6}{\rho S_{BET}} \quad (1)$$

where ρ is the theoretical density (5.031 g cm^{-3}) of yttria[15] and S_{BET} is the specific surface.

The phase identification was investigated by X-Ray diffraction (XRD) using a Cu Kα_1 irradiation (Philips X'pert). The mean grain size was calculated using the Scherrer's formula, and a silicon standard was used to determine the instrumental broadening. Mirror-polished Nd:YAG ceramics (1.6 mm thick) on both surfaces were used to measure optical transmittance by a UV-VIS-NIR spectrometer (Carry 5E, Varian, USA).

3. Results and discussion

Three group of experiments (simply labeled as #1, #2, and #3) were conducted to prepare Nd-doped yttrium carbonate precursors at the yttrium concentration of 0.1 M, 0.3 M and 0.5 M, respectively. From the SEM images of the as-prepared precursors, as shown in Fig. 1a–c, one can see that the low concentration (0.1, 0.3 M) is favor of the formation of small granular and low-agglomerated particles, while the higher concentration leads to irregular and seriously agglomerated particles. The corresponding Nd:Y_2O_3 powders calcined at 1100 °C via a LHS of 600 °C/h, have similar morphologies (Fig. 1d and e), indicating the great dependence of the morphologies of Nd:Y_2O_3 powders on those of the precursors. Particularly, obvious sintering necks are found from the Nd:Y_2O_3 powders of #3, indicating the formation of hard agglomeration of the precursors (Fig. 1c). This agglomerates should be attributed to the over-high solution concentration, which could lead to the compression of the double electrode layer of the colloidal precursors and the formation of strong flocculation and coagulation.[16]

The thermal decomposition of the precursors were studied by TGA-DTG analysis at a heating rate of 180 °C/h, as shown in Fig. 2. The TG curves reveal that the thermal decomposition of the precursors (#1, #2, and #3) completes at ~750 °C with a weight loss of 43.7%, 42.6%, and 42.6% respectively, which approximately equal to the theoretical value (42.66%, calculating from the molecular weight ratio of Y_2O_3 to $Y_2(CO_3)_3{\cdot}2H_2O$). The first peak of the DTG curve (Fig. 2a) is assigned to the removal of the absorbed water. The valley of the DTG curves of the precursors (#1, #2, and #3) corresponds to the temperature of 628 °C, 633 °C and 651 °C, respectively (Fig. 2b), indicating the formation of the intermediate substance. The difference of the temperature between precursor #3 and the other two precursors should be attributed to the thermal hysteresis during the heating process, which arises from the serious agglomeration. Consequently, the whole decomposition process can be divided into three stages by two characteristic temperatures at about 630 °C and 750 °C for precursor #1 and #2, and at about 650 °C and 750 °C for precursor #3, respectively. Based on this analysis, a nonlinear heating schedule (NHS) was suggested as specified below:

Stage 1: from 0 °C to 630 °C (precursor #1 and #2)/650 °C (precursor #3), 600 °C/h;

Stage 2: from 630 °C (precursor #1 and #2)/650 °C (precursor #3) to 750 °C, 100 °C/h;

Stage 3: from 750 °C to 900, 1000, and 1100 °C, 300 °C/h.

In order to verify the best temperature-time condition for crystallization in NHS, XRD patterns of precursors #1 which were calcined to 700 °C and 750 °C without holding time under two heating modes (a LHS at a heating rate of 600 °C/h and the NHS) are investigated. The Nd:Y_2O_3 powders were taken immediately out of the furnace when the calcination schedule was over. From the XRD patterns of Fig. 3, it can be concluded that an amorphous substance formed at temperatures lower than 700 °C and cubic yttria crystallites formed at 750 °C in the LHS, while yttria crystallites form in the temperature zone lower than 700 °C in the NHS. The mean grain sizes (D_{222}) of the powders

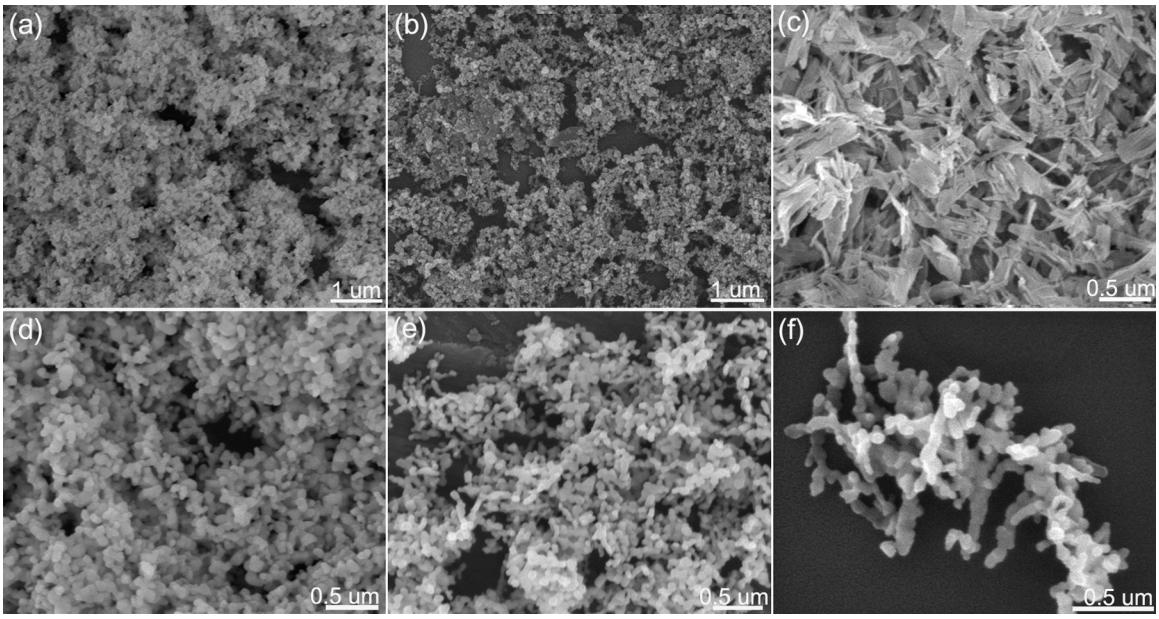

Fig. 1. SEM images of the precursors (a–c) and the corresponding calcined Nd:Y_2O_3 powders (d–f) synthesized at yttrium concentration of 0.1 M, 0.3 M and 0.5 M, respectively.

are 10 nm and 14 nm, corresponding to the LHS and NHS to 750 °C respectively. Based on the results, one can see that the crystallization temperature can be decreased distinctly and better crystallinity can be realized in the NHS.

The SEM images of Nd:Y_2O_3 powders synthesized at yttrium concentration of 0.1 M and calcined at 1100 °C in NHS are provided in Fig. 4. Comparing with the powders synthesized in the LHS (Fig. 1d), the as-prepared Nd:Y_2O_3 powders show good homogeneity in a large scale (Fig. 4a), clear particle contours and less agglomerate bridging (Fig. 4b), indicating a better dispersity. The result illustrates that the NHS can effectively avoid the bridging between neighboring particles. This should be attributed to the better crystallization of Nd:Y_2O_3 grains (as shown in Fig. 3b and d) and the slow rate of their growth in the low temperature region, which can avoid the agglomerate bridging forming effectively in the next high temperature region. As for the LHS, due to the rapid heating the crystallization and the decomposition cannot complete in the low temperature region. As a result, the high-temperature decomposition and crystallization are inevitable, leading to the nonuniform agglomerate bridging.

Since the sintering driving force and the shrinkage inside agglomerates are different from those in between agglomerates, the sintering property of the nanopowders is particularly sensitive to the agglomerates of the nanoparticles.[5] For the fabrication of transparent ceramics, it is crucial to prepare well sinterable nanopowders with small particle size, low-agglomeration, and narrow PSD. Here we define a parameter to evaluate the aggregation degree of the powders,

$$N = \left(\frac{D_{\mathrm{BET}}}{D_{\mathrm{XRD}}}\right)^3 \tag{2}$$

where D_{XRD} is the mean grain size which is calculated using the Scherrer's formula, D_{BET} is the equivalent particle size. The parameter N gives an approximation of the average number of

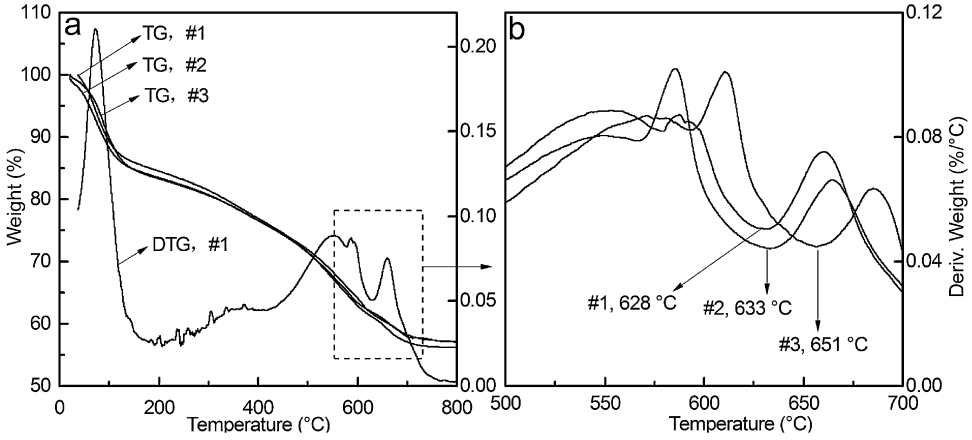

Fig. 2. TGA curves (a) of the precursors and the corresponding magnified DTG curves (b).

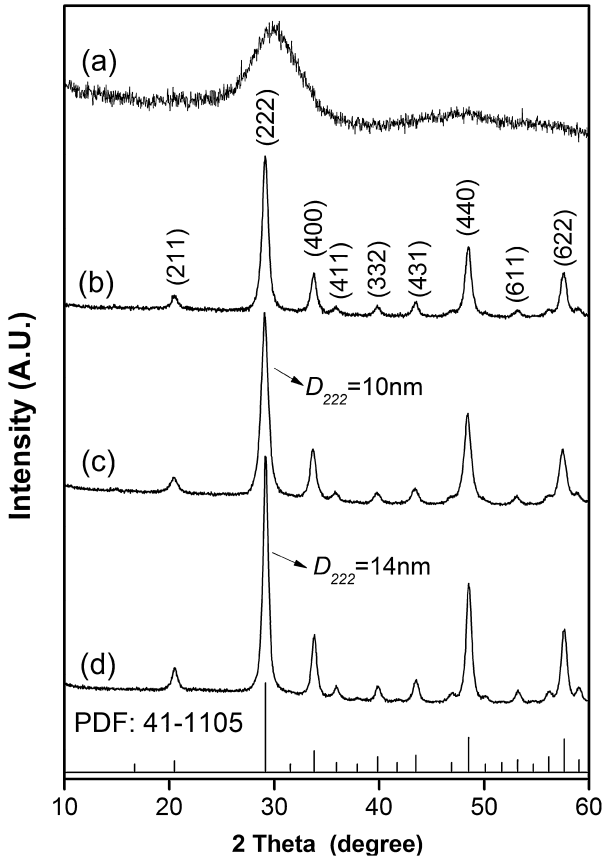

Fig. 3. XRD patterns of Nd:Y_2O_3 powder #1 calcined in (a) LHS to 700 °C, (b) NHS to 700 °C, (c) LHS to 750 °C and (d) NHS to 750 °C.

the primary particles in the aggregates. The dispersity of the Nd:Y_2O_3 powder can be reflected in the *N* value, and the smaller the *N*, the better the dispersity.

Table 1 shows the variation of parameter *N* with the calcination temperature for the powders (#1) under two heating modes. The *N* value increases with the increasing temperature, and the relatively lower *N* values are obtained in the NHS, which implies the less primary particles in the aggregates. Meanwhile, as shown in Fig. 5a, the range of pore size did not vary with the calcination mode and temperature, but a larger proportion of the pores in the range of 20–120 nm were obtained in the LHS. The more micro-pores inside the aggregates will result in the nonuniform compaction, which will cause the different shrinkages and shrinkage rates inside and in between agglomerates during the sintering process.[17]

Table 1
The *N* value of the calcined Nd:Y_2O_3 powders synthesized from 0.1 M [Y^{3+}].

	N value		
	900 °C	1000 °C	1100 °C
LHS	2.7	3.8	8.1
NHS	2.6	3.4	6.9

Powders with a small particle mean size and a narrow PSD are conducive to achieving the best particles packing with the smallest pore size and the narrowest pore size distribution, which could conduce to preventing the pore-boundary separation and making full dense ceramics.[18] The PSD of the Nd:Y_2O_3 nanopowders calcined at 900, 1000 and 1100 °C in the LHS, have similar trends, as shown in Fig. 5b. When the yttrium concentration of 0.1 M was employed in synthesis, the PSD curves of the powders (#1) change from double peaks to single peak and the mean particle size increases slowly from 260 nm to 320 nm, with the increasing calcination temperature. Similarly, the Nd:Y_2O_3 powders (#2) synthesized from 0.3 M yttrium have mean particle size of 120 nm, 200 nm, and 300 nm, corresponding to the calcination temperature of 900, 1000 and 1100 °C, respectively. The growing mean particle size should be resulted from the increasing agglomeration with the temperature, in agreement with changes of the *N* values (as listed in Table 1). In contrast, when yttrium concentration equals 0.5 M, the obtained powders (#3), show a narrow PSD and small mean size (~200 nm) at 900 °C, while a broader PSD and larger mean particle size (~300 nm) are obtained at the higher temperature. The broadened PSD should be attributed to the formation of a large amount of sintering-necks at the high temperature (as shown in Fig. 1f).

Fig. 5c presents the PSD of the Nd:Y_2O_3 powders synthesized at 1100 °C in the two calcination modes. As illustrated in the figure, one can see that the powders (#1) have a relatively smaller mean size and a narrower PSD in the range of 100–300 nm via the NHS. The PSD of sample #2 shows that the larger particles (>220 nm) take a relatively small proportion via

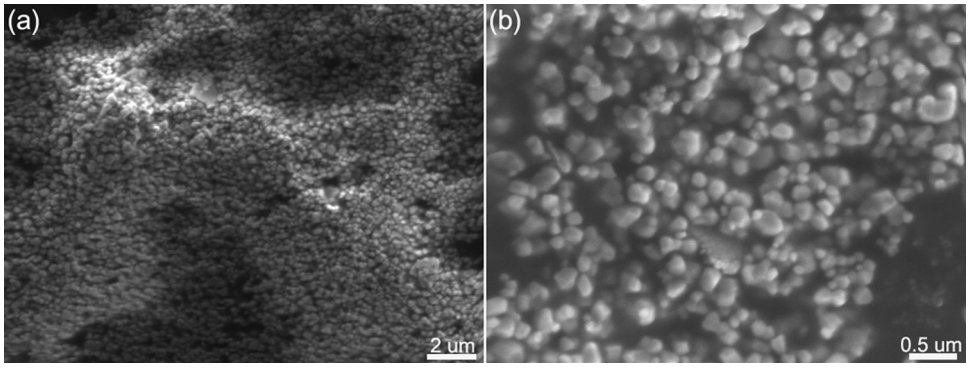

Fig. 4. SEM images of Nd:Y_2O_3 powder #1 calcined at 1100 °C for 4 h in (a) NHS and (b) a magnified image of (a).

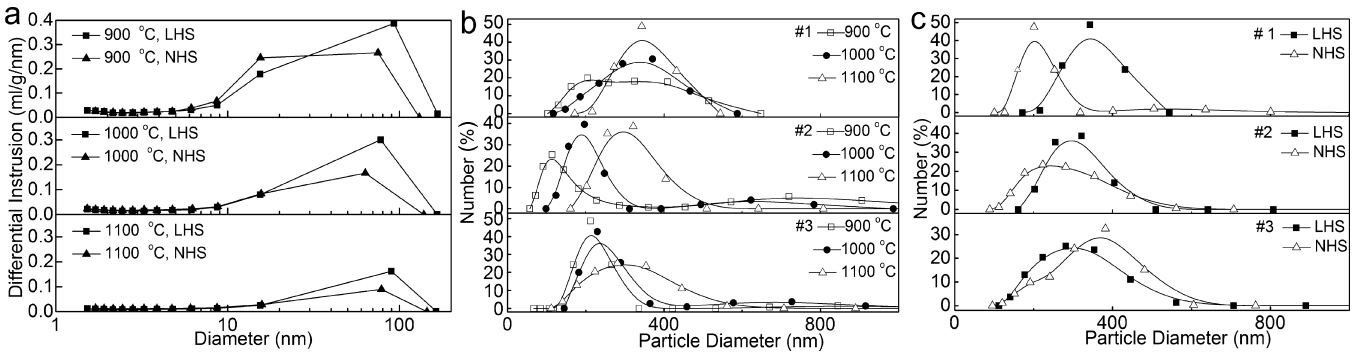

Fig. 5. (a) Pore size distribution curves of the Nd:Y_2O_3 powders #1 calcined in LHS and NHS; PSD curves of Nd:Y_2O_3 nanopowders #1, #2 and #3 calcined at (b) different temperatures in LHS, and under (c) different heating modes at 1100 °C.

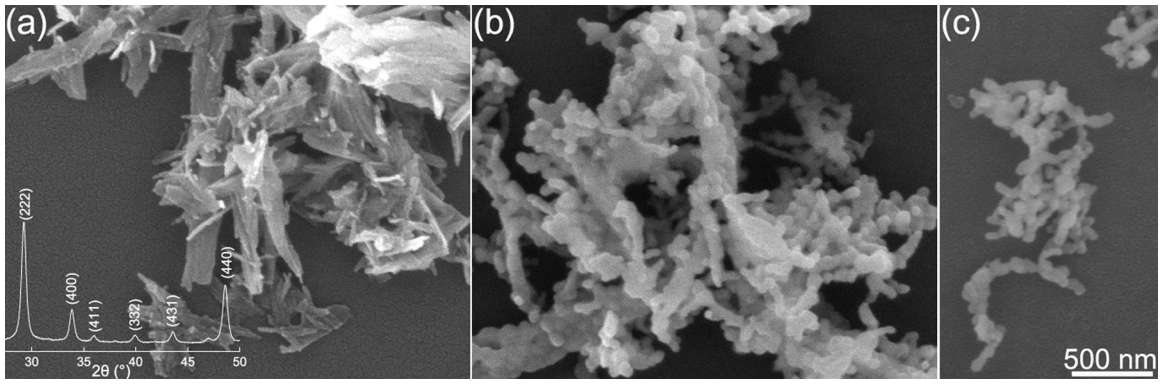

Fig. 6. The same magnification SEM images of the powders #3 calcined in NHS at (a) 750 °C and (b and c) 1100 °C, respectively; the inset in (a), XRD pattern of the corresponding powders.

the NHS, indicating the superiority of the NHS for synthesizing dispersed nanopowders.

However, the PSD of sample #3 shows that a larger mean particle size is obtained via the NHS (as shown in Fig. 5c), which is in contrast to former two samples. To clarify the abnormal effect of the NHS on the PSD of the powders (#3), we examined the morphology evolution of the powders (#3) calcined in the NHS. Fig. 6 shows the morphologies and dispersion states of Nd:Y_2O_3 powders synthesized via NHS at 750 °C and 1100 °C, respectively. It is clear that, after calcination at 750 °C in NHS, the powders show not only better crystallinity (the inset in Fig. 6a, JCPDS, No. 41-1105) but also serious agglomeration (Fig. 6a), which is analogous to the morphology of the precursor (as shown in Fig. 1c). Though the powders decompose to nanoparticles when calcined at 1100 °C, agglomerates consisting of interconnected particles are obtained (as shown in Fig. 6b and c). The result indicates that the agglomerates are inherited from the agglomerated precursors (#3) and have formed at the low temperature. Generally, for the seriously agglomerated precursors, the crystallization and sintering process overlap each other at the low temperatures and cannot be distinguished clearly, and thus it is infeasible to control the evolution processes of microstructures independently by tuning the calcination parameters. In other words, one cannot avoid particle agglomeration at the high temperatures whether the NHS or the LHS are used, for they cannot break the agglomerates into dispersed nanoparticles. In this case, the agglomeration of the powders is strongly dependent on the duration of calcination at high temperatures.

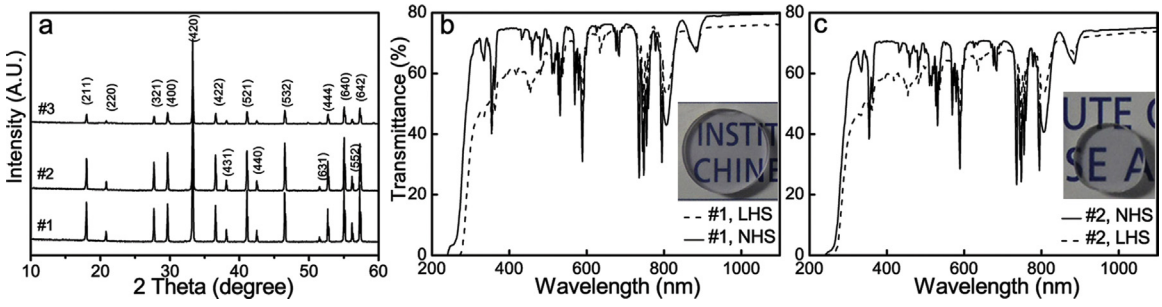

Fig. 7. (a) XRD patterns of the sintered Nd:YAG ceramics with the obtained Nd:Y_2O_3 powders. (b and c) Transmittance spectra of the mirror-polished Nd:YAG ceramics (1.6 mm thick).

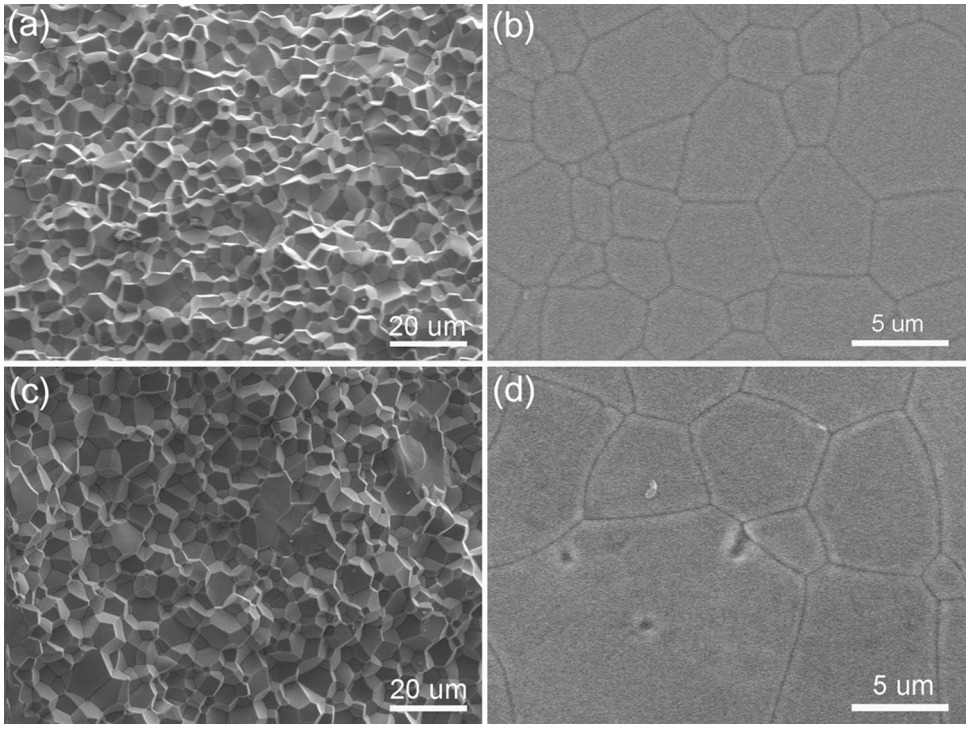

Fig. 8. SEM images of the fracture surface and the mirror-polished surface of the Nd:YAG transparent ceramics using Nd:Y_2O_3 powders #1 calcined in NHS (a and b) and LHS (c and d), respectively.

Specially, in comparison to the LHS the longer heating time of the NHS (due to the slow heating rate) during the crystallization process exacerbate the agglomeration at the low temperature, as shown in Fig. 5c (#3).

XRD patterns of the Nd:YAG ceramics are demonstrated in Fig. 7a. It could be seen that pure YAG phase can be obtained by using the as-prepared Nd:Y_2O_3 powders, and no impurities are detected in all of the ceramics (Fig. 7a). From the transmittance spectra of mirror-polished Nd:YAG ceramics, we can see that well-dispersed granular Nd:Y_2O_3 nanopowders (#1 and #2) conduce to excellent transparency (Fig. 7b,c). The transmittances of the ceramics are all above 73% at lasing wavelength of 1064 nm. Furthermore, Nd:YAG ceramics employing the Nd:Y_2O_3 powders calcined in the NHS, show higher transmittance values (74.9% of #1 and 70.7% of #2 at wavelength of 400 nm) than those in the LHS (60.9% of #1 and 59.7% of #2 at wavelength of 400 nm), indicating that the NHS is more conducive than LHS to the densification of ceramics.

Fig. 8 illustrates the SEM images of the fracture surface and the mirror-polished surface of the Nd:YAG transparent ceramics using Nd:Y_2O_3 powders (#1) calcined in NHS and LHS, respectively. It could be seen that the average grain sizes both were about 5 um and the fracture modes of the ceramics were mainly intergranular. The Nd:YAG ceramic with the Nd:Y_2O_3 powder calcined in NHS exhibited a nearly pore-free structure (Fig. 8b), while the ceramic with the Nd:Y_2O_3 powder calcined in LHS showed a large grain and a small quantity of residual pores in the grain and at the boundary (Fig. 8d). The abnormal grain growth should be due to the existence of large original particles in the Nd:Y_2O_3 powders obtained via LHS, indicating that the powders with a narrow PSD are necessary to fabricate transparent ceramics.

4. Conclusions

Nanostructured Nd:Y_2O_3 powders have been synthesized by the co-precipitation method. The results indicate that the morphology of the Nd:Y_2O_3 particle is strongly related to that of the precursor, which is influenced by the initial solution concentration. The precursors were calcined by two different calcination modes, nonlinear and linear heating schedules (NHS and LHS). The NHS shows a particular superiority to the LHS on the synthesis of well-dispersed nanopowders with a narrow PSD from the well-dispersed precursors. Studies on the precursor decomposition confirm that the crystallization temperature can be reduced substantially in NHS, which can lighten the high-temperature agglomeration. Nevertheless, for the serious agglomerated precursors, the hard agglomerates inheriting from the precursors have formed at the low temperature of crystallization process, and thus it is infeasible to control the evolution processes of microstructures independently by tuning the calcination parameters. By using the dispersed Nd:Y_2O_3 powders calcined in LHS and NHS, transparent Nd:YAG ceramics were fabricated through the solid state reaction in vacuum. The result show that Nd:YAG ceramics corresponding to the NHS route have higher optical transmittances and less residual pores than those corresponding to the LHS.

Acknowledgments

We would like to thank the financial support from the National Natural Science Foundation of China (Nos. 50972146 and 51101150).

References

1. Ikesue A, Kinoshita T, Kamata K, et al. fabrication and optical-properties of high-performance polycrystalline Nd-Yag ceramics for solid-state lasers. *J Am Ceram Soc* 1995;**78**:1033–40.
2. Appiagyei KA, Messing GL, Dumm JQ. Aqueous slip casting of transparent yttrium aluminum garnet (YAG) ceramics. *Ceram Int* 2008;**34**:1309–13.
3. Zhang J, An LQ, Liu M, et al. Sintering of Yb^{3+}:Y_2O_3 transparent ceramics in hydrogen atmosphere. *J Eur Ceram Soc* 2009;**29**:305–9.
4. Ikesue A, Aung YL. Ceramic laser materials. *Nat Photonics* 2008;**2**:721–7.
5. Ragulya AV. Consolidation of ceramic nanopowders. *Adv Appl Ceram* 2008;**107**:118–34.
6. Durán P, Tartaj J, Moure C. Sintering behaviour of Y_2O_3 powders prepared by the polymer complex solution method. *Ceram Int* 2002;**28**:791–803.
7. Dupont A, Largeteau A, Parent C, et al. Influence of the yttria powder morphology on its densification ability. *J Eur Ceram Soc* 2005;**25**:2097–103.
8. Tanner PA, Fu LS. Morphology of Y_2O_3: Eu^{3+} prepared by hydrothermal synthesis. *Chem Phys Lett* 2009;**470**:75–9.
9. Jeong JY, Park SW, Moon DK, et al. Synthesis of Y_2O_3 nano-powders by precipitation method using various precipitants and preparation of high stability dispersion for backlight unit (BLU). *J Ind Eng Chem* 2010;**16**:243–50.
10. Mouzon J, Nordell P, Thomas A, et al. Comparison of two different precipitation routes leading to Yb doped Y_2O_3 nano-particles. *J Eur Ceram Soc* 2007;**27**:1991–8.
11. Ikegami T, Li JG, Mori T, et al. Fabrication of transparent yttria ceramics by the low-temperature synthesis of yttrium hydroxide. *J Am Ceram Soc* 2002;**85**:1725–9.
12. Vasylkiv O, Sakka Y, Borodians'ka H. Nonisothermal synthesis of yttria-stabilized zirconia nanopowder through oxalate processing: II, morphology manipulation. *J Am Ceram Soc* 2001;**84**:2484–8.
13. Ragulya AV, Vasylkiv OO, Skorokhod VV. Synthesis and sintering of nanocrystalline barium titanate powder under nonisothermal conditions, 1. Control of dispersity of barium titanate during its synthesis from barium titanyl oxalate. *Powder Metall Met Ceram* 1997;**36**:170–5.
14. Wen L, Sun X, Xiu Z, et al. Synthesis of nanocrystalline yttria powder and fabrication of transparent YAG ceramics. *J Eur Ceram Soc* 2004;**24**:2681–8.
15. Gong H, Tang DY, Huang H, et al. Effect of grain size on the sinterability of yttria nanopowders synthesized by carbonate-precipitation process. *Mater Chem Phys* 2008;**112**:423–6.
16. Dalmaschio CJ, Ribeiro C, Leite ER. Impact of the colloidal state on the oriented attachment growth mechanism. *Nanoscale* 2010;**2**:2336–45.
17. Hsieh H-L, Fang T-T. Effect of green states on sintering behavior and microstructural evolution of high-purity barium titanate. *J Am Ceram Soc* 1990;**73**:1566–73.
18. Messing GL, Stevenson AJ. Toward pore-free ceramics. *Science* 2008;**322**:383–4.